2022 IEEE 5th International Conference on Soft Robotics (RoboSoft)
April 4-8, 2022, Edinburgh, UK

A Magnetically-Actuated Flexible Capsule Robot for Untethered Cardiovascular Interventions

Gijsbert Michiel van Vliet, Sarthak Misra, Venkatasubramanian Kalpathy Venkiteswaran

***Abstract*— Robotic medical systems have been developed over the last few decades to reduce invasiveness and increase possibilities of minimally invasive surgery (MIS). This paper investigates a new, wireless, magnetically-actuated capsule robot as an untethered tool for cardiovascular surgery. The compliant magnetic capsule robot (CMCR) is designed to navigate larger blood vessels such as the abdominal aorta. Circular flexures provide the CMCR with radial adaptability, and the radial stiffness is analyzed using beam theory to calculate the actuation torque. Axial flexibility is also endowed onto the CMCR using a segmented structure and soft material core. Magnets are embedded on the CMCR to allow wireless actuation. Experiments are performed on prototypes of the CMCR to demonstrate its function as a proof-of-concept. Controlled actuation and adaptability of the CMCR are demonstrated in straight and curved tubes of varying diameters. Actuation of the CMCR in fluid flow and an approach for MIS insertion are also demonstrated to validate its potential for clinical application.**

I. Introduction

Minimally invasive surgery (MIS) has emerged as an indispensable approach in many surgical disciplines [1], and the advent of robotic surgical devices has expanded the scope and impact of MIS [2], [3]. Recently, the development of robotic devices for surgery has evolved from large rigid platforms towards small, task-specific flexible robots. This improves accessibility to delicate and confined areas in the body which were previously difficult or impossible to reach [4].

Within surgical robotic devices, tethered continuum robots show some favorable MIS characteristics, such as their compliance and the ability to navigate narrow passages [5]–[7]. These properties are utilized in MIS tools like tendon-driven concentric tube robots [8] and magnetic sub-millimeter-diameter guidewires [9]. Nevertheless, tethered devices are limited in maneuverability and are not able to reach and perform surgical tasks in many areas within the body with restricted access [10].

As an alternative to tethered systems, mobile untethered capsule devices have been investigated to reach remote sites in the human body in even less invasive ways. Commercialized wireless capsule endoscopes (e.g., Pillcam®, Medtronic, USA and MiroCam®, IntroMedic Co.,Ltd., South Korea) have already been accepted in clinics for diagnosis of gastrointestinal diseases [11]–[13]. The clinical functionality of these capsule endoscopes has recently been expanded through the introduction of magnetically-actuated capsule endoscopes (MACEs) which allow active control of the capsule, although they are as yet are unable to perform surgical interventions [14], [15] (NaviCam®, AnX Robotica Corp., USA).

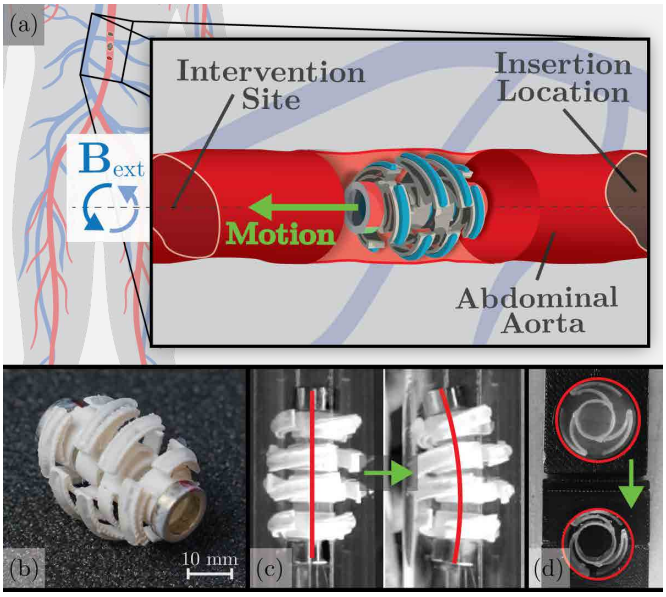

Fig. 1: Overview of the Compliant Magnetic Capsule Robot (CMCR). (a) Conceptual sketch of CMCR moving between the insertion and intervention sites in the abdominal aorta under the influence of a rotational external magnetic field ($\mathbf{B}_{ext}$). (b) Prototype of the CMCR. (c) The CMCR has axial flexibility which allows it to bend along its long axis and move through curved vessels. (d) Radial compressibility of the CMCR ensures it maintains contact with the vessel wall when moving through sections of varying diameter.

Magnetic actuation has benefits including human-safe operation, wireless actuation and rapid response, and has been investigated for medical applications such as magnetic catheter ablation and electromagnetic navigation bronchoscopy [16], [17]. Untethered soft robots controlled using magnetic fields have demonstrated motion in fluids, manipulate objects in the workspace, and the ability to carry cargo [18]–[20]. Magnetic capsule robots capable of fine-needle biopsy have been developed by combining the benefits of magnetic actuation and soft materials, demonstrating potential for real clinical application [21].

Existing capsule endoscopes focus primarily on the digestive tract [22], [23], including MACEs which allow

All authors are affiliated with Surgical Robotics Laboratory, Department of Biomechanical Engineering, University of Twente, 7500 AE Enschede, The Netherlands. Contact: v.kalpathyvenkiteswaran@utwente.nl

S. Misra is also affiliated with the Department of Biomedical Engineering, University of Groningen and University Medical Centre Groningen, 9713 GZ Groningen, The Netherlands.

This research has received funding from the Faculty of Engineering Technology at the University of Twente under the project 'Symbiobot'.

2022 IEEE 5th International Conference on Soft Robotics (RoboSoft) | 978-1-6654-0828-8/22/$31.00 ©2022 IEEE | DOI: 10.1109/ROBOSOFT54090.2022.9762151

active control of the orientation of the capsule using an external magnetic field. Previous research in rigid magnetic capsule robots has considered the use of screw-like motion for controlled motion in air and liquids [24], [25]. However, existing capsule robots lack the ability to navigate vasculature and simultaneously maintain their position within blood vessels to perform surgical tasks in the face of blood flow. It would be beneficial to have robotic capsules that can passively anchor to the blood vessel at a target location, withstanding blood flow while having capabilities to perform surgical interventions.

This paper investigates the design of an untethered capsule robot for interventions in the cardiovascular system (Fig. 1). The compliant magnetically-actuated capsule robot (CMCR) has radial adaptability and stiffness (through curved flexures) to maintain contact with the vessel wall and remain stationary in the face of blood flow. It can be moved along blood vessels of varying diameters using rotating magnetic fields, utilizing a screw-like motion. A segmented structure with a soft material core endows the CMCR with axial flexibility for traversing curved paths. The flexibility of the CMCR can be tuned based on actuation requirements, and it can be inserted in its compressed state for minimally invasive entry during operation. The feasilibty of the CMCR is demonstrated as a proof-of-concept for capsule robots towards cardiovascular interventions.

II. Compliant Magnetic Capsule Design

In this section, the design of the CMCR is explained in detail. Three attributes — passive radial adaptability, axial flexibility, and active magnetic actuation for movement — are explained. This is followed by an explanation of the fabrication process. An overview of the design and its dimensions can be found in Fig. 2 and Table I.

A. Radial Adaptability

The capsule robot requires a radially adaptable structure to adjust to the fluctuating diameter of blood vessels. This adaptability is achieved through flexures. Two circular flexures are connected in series to form a flexure pair that provides compliance in the radial direction. One end of the inner flexure is connected to the core, while the outer flexure presses against the vessel wall. The flexure-pairs allow the CMCR to decrease its diameter in small blood vessels under the compressive force from the vessel wall, and expand in larger vessels due to the elasticity of the flexures.

B. Axial Flexibility

Flexibility in the axial direction of the CMCR is necessary for moving through curved blood vessels. Segmentation of the capsule structure and use of a soft material core allow axial bending of the CMCR. Each segment of the capsule structure consists of circular flexure pairs arranged in groups of three. The soft material core connects these segments while allowing relative bending between them.

C. Magnetically-Actuated Movement

The CMCR should move steadily through the blood vessel using magnetic actuation. Rotation-based screw-like motion under the influence of a rotating magnetic field is utilized for this motion. To this end, two radially-magnetized permanent magnets are embedded in the CMCR. These magnets create an internal magnetic dipole (μ_{int}) along a radial direction which aligns with an external magnetic field ($\mathbf{B}_{\text{ext}}$) (Fig. 2c). Therefore, rotation of the CMCR is induced when the external field is rotated around the longitudinal axis of the CMCR. This rotational motion is transferred to longitudinal motion through the outer circular flexures which form a helical thread with a 10° pitch angle.

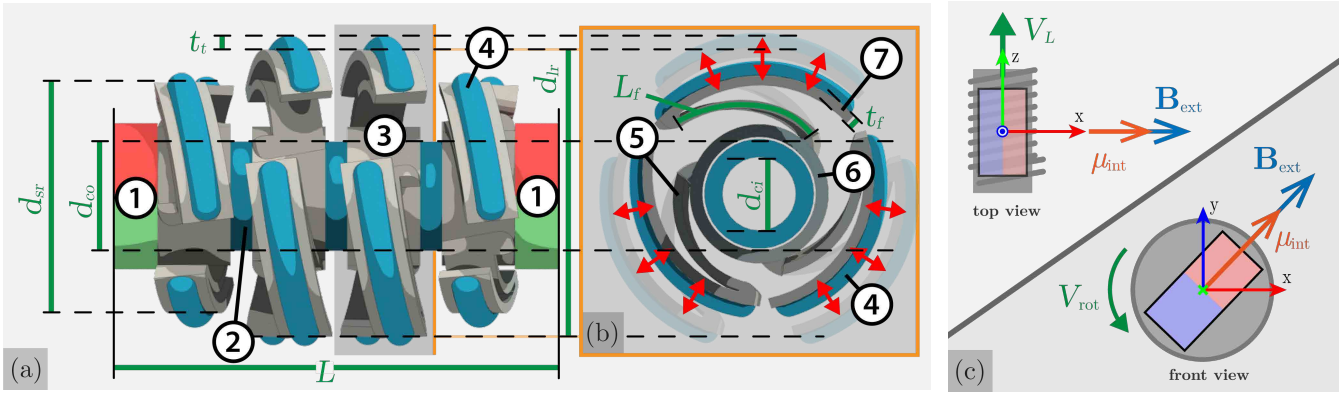

Fig. 2: Design of the compliant magnetic capsule robot (CMCR). (a) Side view of the CMCR and its dimensions: Total capsule length (L), flexible thread thickness (t_t), flexure thickness (t_f), flexure length (L_f), large ring OD (d_{lr}), small ring OD (d_{sr}), flexible core OD (d_{co}), and flexible core ID (d_{ci}). The capsule design contains: ① permanent magnets, ② a flexible core, and ③ segments of flexure pairs. (b) Front view of the CMCR showing compression of the flexure pairs and passive elastic restoration to the default diameter. The flexure pairs consist of an inner flexure ⑤ and an outer flexure ⑦ in series. A flexible thread ④ is attached to the outer flexure to ensure soft contact with the vessel wall. The inner part of the segment is a rigid core ⑥. (c) Working principle for the CMCR: The internal magnetic dipole of the robot (μ_{int}) aligns with the external magnetic field ($\mathbf{B}_{\text{ext}}$). Forward (or backward) motion (V_L) is caused by screw-like rotational motion (V_{rot}) due to the rotation of the external field.

TABLE I: Dimensions of the three different scaled prototypes of the compliant magnetically-actuated capsule robot (CMCR).

Dimension	Symbol	Prototype scale 1.00	1.25	1.50
Uncompressed OD (mm)				
- Large ring	$d_{lr,u}$	20.0	24.8	30.4
- Small ring	$d_{sr,u}$	16.0	19.8	24.3
Compressed OD (mm)				
- Large ring	$d_{lr,c}$	15.0	18.6	22.8
- Small ring	$d_{sr,c}$	12.0	14.9	18.3
Flexure length (mm)				
- Large ring	$L_{f,lr}$	10.0	12.5	15.0
- Small ring	$L_{f,sr}$	5.5	6.9	8.3
Flexure thickness (mm)	t_f	0.7	0.7	0.7
Flexible core OD (mm)	d_{co}	7.5	9.3	11.4
Flexible core ID (mm)	d_{ci}	5.0	6.2	7.6
Flexible thread thickness (mm)	t_t	1.0	1.2	1.5
Total capsule length (mm)	L	30.5	37.7	49.2

D. Prototype Fabrication and Scaling

Prototypes of the CMCR are fabricated using a combination of rapid prototyping techniques. The segments with the flexure-pairs are 3D printed with ABSplus P430 material on the Fortus 250mc FDM printer (Stratsys, Ltd., Eden Prairie, MN, USA). All circular flexures have an arc angle of 90°and a thickness (t_f) of 0.7 mm, which was the lowest possible thickness using the 3D printer. The core is 3D printed with Elastic 50A Resin on a Form 2 stereolithography (SLA) printer (Formlabs, Somerville, MA, USA). Elastic 50A Resin is used for these threads to improve the robot's compliance to the tissue of the aortic wall. The threads have a thickness (t_t) of 1 mm and are glued to the flexure-pairs.

Three different scaled prototypes of the CMCR design are fabricated to test the performance with respect to stiffness of the circular flexures. A base prototype (1.00×) is created with an uncompressed outer diameter of 20 mm which would be suitable for the abdominal aorta. For the other prototypes, the thickness of the flexures (t_f) is kept constant and the other dimensions are scaled to 1.25× and 1.50× of the base design. The dimensions of all the prototypes can be found in Table I. In the base design, two 10/7x3 mm radially-magnetized ring magnets (Model R-10-07-03-DN, Supermagnete, Gottmadingen, Germany) are embedded in the CMCR. Two 12x6 mm disc magnets with a radial N42 magnetisation (Model S-12-06-DN, Supermagnete, Gottmadingen, Germany) are used for the 1.25× and 1.50× scale prototypes.

III. Modeling Flexure Stiffness

The radial stiffness of the CMCR determines its adaptability to changing vessel diameters and the actuation field necessary to generate motion. In this section, a mathematical model is derived to calculate the stiffness of the flexure pairs on the CMCR.

A single flexure-pair of the capsule robot is modeled as two circular cantilever beams connected in series (Fig. 3a). The outer beam is in contact with the vessel wall, and therefore it is assumed that a distributed force ($\bar{F}$) acts per unit length on the outer beam. The inner beam is fixed at the

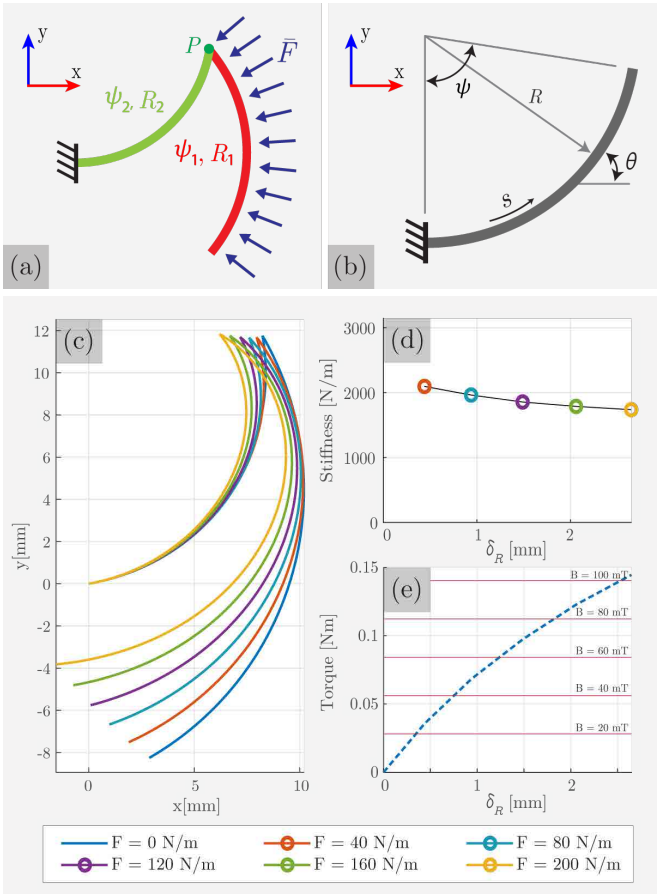

Fig. 3: Stiffness modeling of flexure pairs. (a) The outer flexure experiences a distributed force per unit length ($\bar{F}$), has undeflected radius (R_1) and subtends an arc angle (ψ_1). The inner flexure is fixed at the root, has undeflected radius (R_2) and subtends an arc angle (ψ_2). (b) The deflection of each flexure is calculated using beam theory, with s representing the independent coordinate along the beam length, and $\theta(s)$ the deflected orientation of the beam at s. (c) Shapes of the 1.50× scale flexure pairs under increasing load. (d) Stiffness of the flexure pair under increasing radial deformation (δ_R). (e) Comparison of stall torque due to friction under increasing radial deformation and maximum torque produced by a magnetic field.

root and the reaction loads from the outer beam act at the tip of the inner beam. For simplicity, only planar deflections (in the xy-plane as indicated in Fig. 3a) are considered.

For a single beam, the deflection can be characterized using beam theory assuming bending-dominant behavior. Each beam is defined by its radius R and arc angle ψ, with arc length $L = \psi R$. The independent centerline coordinate $s \in [0, L]$ and the coordinate-dependent slope $\theta(s)$ are used to calculate the deflected shape using beam theory as

$$\theta'(s) = \frac{M(s)}{EI} + \frac{1}{R}, \tag{1}$$

with bending moment $M(s)$, second moment of area I and elastic modulus E. For a rectangular cross-section, $I = wt^3/12$ with width w and thickness t.

For the analysis here, each beam is considered independently, with the deflection and reaction loads on the outer beam calculated first, followed by the inner beam.

Following the methodology described by Venkiteswaran and Su [26], Eqn. (1) is differentiated with respect to the variable s and combined with two boundary conditions to obtain a set of equations that define beam behavior.

For the outer beam, the derivative of the bending moment in the z-direction is calculated as

$$dM_1^z(s) = ||\mathbf{s}^* \times \mathbf{dF}||, \tag{2}$$

where

$$\mathbf{dF} = \bar{F} \cdot \begin{bmatrix} -\sin(\theta_1(s)) \\ \cos(\theta_1(s)) \end{bmatrix}, \tag{3}$$

and

$$\mathbf{s}^* = \begin{bmatrix} \int_s^L \cos\theta_1(s)ds \\ \int_s^L \sin\theta_1(s)ds \end{bmatrix}. \tag{4}$$

For planar deflections in the xy-plane, only the z-component of the bending moment acts on the beam. Therefore,

$$\theta_1''(s) = \frac{-dM_1^z(s)}{EI}. \tag{5}$$

For the outer beam, the slope at the fixed end ($s = 0$) is zero. At the end of the beam ($s = L$), the moment $M_1^z(L_1)$ is zero. Therefore, the boundary conditions are

$$\theta_1(0) = 0, \qquad \theta_1'(L_1) = \frac{1}{R_1}. \tag{6}$$

For the inner beam, the reaction force $\mathbf{F}_P$ and reaction moment M_P^z at the connection point P (Fig. 3a) between the two beams must be calculated first. This force and moment are defined as

$$\mathbf{F}_P = \int_0^{L_1} \mathbf{dF} ds = \bar{F} \cdot \int_0^L \begin{bmatrix} -\sin(\theta_1(s)) \\ \cos(\theta_1(s)) \end{bmatrix} ds, \tag{7}$$

and

$$M_P^z = M_1^z(0). \tag{8}$$

Thus, for the inner beam,

$$\theta_2''(s) = \frac{-dM_2^z(s)}{EI} = \frac{1}{EI}\left(F_P^x \sin\theta_2(s) - F_P^y \cos\theta_2(s)\right). \tag{9}$$

The slope at the fixed end of the beam ($s = 0$) is zero. The moment M_P acts at the other end of the beam ($s = L$). This results in the boundary conditions

$$\theta_2(0) = 0, \qquad \theta_2'(L_2) = \frac{M_P^z}{EI} + \frac{1}{R_2}. \tag{10}$$

Eqns. (5),(6),(9) and (10) form a set of differential equations and boundary conditions can be solved using numerical methods. The shape of the deflected beams can be calculated from the x and y coordinates as

$$x(s) = \int_s^L \cos\theta(s)ds \tag{11}$$

$$y(s) = \int_s^L \sin\theta(s)ds. \tag{12}$$

With these deflected beam shapes the mean change in radius (δ_R) of the flexure-pair is calculated across 10 points along the length of the outer beam. For a given input force $F = L_1\bar{F}$, the stiffness of the flexure-pair k_{fp} is defined as

$$k_{fp} = F/\delta_R \ . \tag{13}$$

The reaction force from compression of the flexure pairs leads to friction between the CMCR and vessel wall. If N flexure pairs under radial compression δ_R are in contact with the vessel wall, the stall torque is given by

$$T_f = \mu_f N k_{fp}\ \delta_R\ (R - \delta_R), \tag{14}$$

where μ_f is the coefficient of static friction between the CMCR and vessel wall. The CMCR is able to overcome the friction stall torque and move under an external magnetic field $\mathbf{B}_{\text{ext}}$ if

$$T_f < T_B = ||\mu_{\text{int}} \times \mathbf{B}_{\text{ext}}||, \tag{15}$$

where μ_{int} is the total magnetic dipole moment of the CMCR and T_B is the induced magnetic torque.

The above condition can be used to determine the magnetic field necessary to move the CMCR. As an example, this is evaluated for one of the prototypes (1.50× scale) and tested under a uniform magnetic field (Sec. IV). The parameters for the analysis are given in Table II. The coefficient of friction is assumed to be 0.8 for contact between the flexible thread made of rubber and the acrylic wall of the tubes used for experiments. The deflection of the flexure-pair is obtained for a range of $\bar{F} \in [0, 200]$ N/m (Fig. 3c). It is noticeable that most of the deformation is concentrated on the outer flexure. The stiffness of the flexure-pairs decreases under deformation, as can be seen in Fig. 3d. The comparison between maximum magnetic torque and friction stall torque is given in Fig. 3e. For the 1.50× scale prototype, a magnetic field of 100 mT can move the CMCR under 2.5 mm radial compression.

TABLE II: Parameters for stiffness and actuation analysis for the 1.50× scale prototype.

Parameter	Value	Parameter	Value
Elastic modulus E (GPa)	2.20	Friction coefficient μ_f	0.80
Flexure width w (mm)	5.30	Flexure thickness t (mm)	0.70
Flexure 1 radius R_1 (mm)	14.7	Flexure 2 radius R_2 (mm)	10.2
Flexure Angle ψ (deg)	90.0	Magnet dipole μ_B (Am^2)	1.46

IV. Experiments and Results

Experiments are performed on the prototypes to demonstrate the motion of the CMCR under a rotating magnetic field, and also its radial adaptability, axial flexiblity and potential for application in minimally invasive surgery. (**Please refer to the Supplementary Video**).

A. Motion experiments

The motion of the CMCR is tested in tubes of different shapes. The magnetic field in these experiments is generated with a Ø60 mm N42 disc magnet (Model S-60-05-DN, Supermagnete, Gottmadingen, Germany). Tubes of different inner diameter (ID) are used to demonstrate motion in various states of radial compression of the CMCR, and all three scaled prototypes are tested.

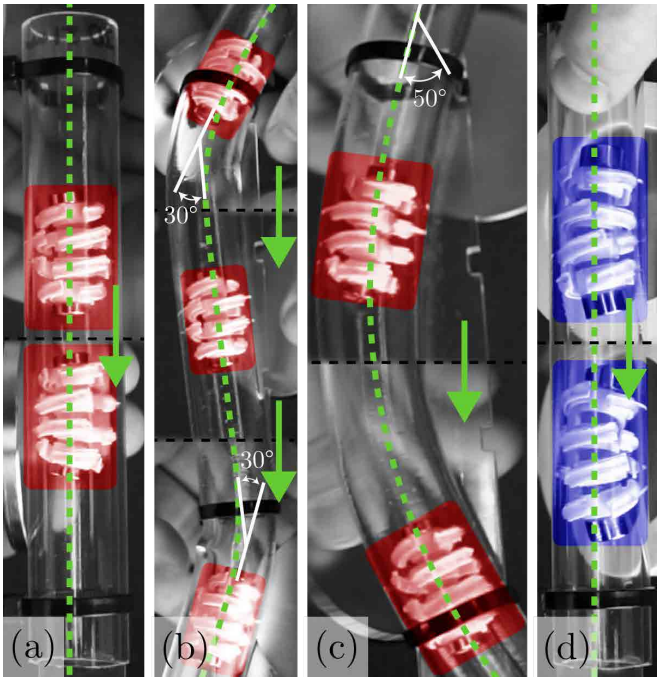

Fig. 4: Motion experiments with a handheld disc magnet: 1.00× scale prototype (uncompressed) in a tube of inner diameter 21 mm for (a) straight-line motion, (b) motion through S-shape with 30° bends, and (c) motion through 50° curve. (d) 1.25× scale prototype (compressed) in tube of 21 mm inner diameter demonstrating straight-line motion.

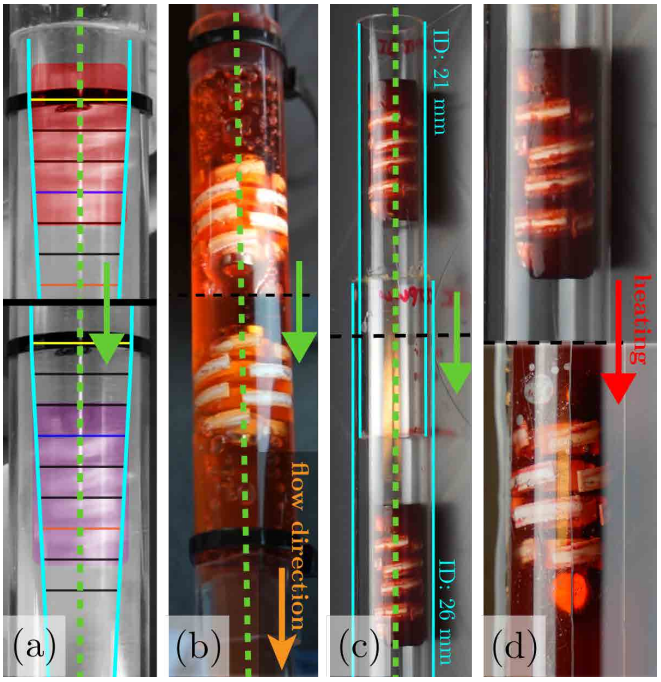

Fig. 5: (a) Motion of compliant magnetic capsule robot (CMCR) in a tapered tube from an uncompressed state (red box) up to a partly compressed state (purple box). (b) Motion test in the fluid flow. (c) Insertion of the compressed CMCR encapsulated in ice from inner diameter (ID) 21 mm tube to ID26 mm tube. (d) Releasing CMCR from ice using water to expand to 26 mm.

Figure 4 shows results from these experiments. The CMCR moves due to the rotation induced by the external magnetic field in compressed and uncompressed states. The different prototypes are initially tested in straight tubes, followed by a tube with an S-shape with two sharp 30° bends and another tube has a gradual 50° circular curve. In all experiments, the CMCR is able to move forward and backward by reversing the direction of rotation of the magnet. However, slippage is occasionally observed due to attractive forces from the disc magnet.

In addition, some experiments are executed in a setup with electromagnets (BigMag [27]) to test the performance of the capsule robot in controlled magnetic fields up to 50 mT. The motion of different scaled prototypes of CMCR is tested in straight tubes at different states of compression. It is observed that the 1.50× prototype moves under the generated magnetic field (up to 50 mT) in partially compressed states, tallying with the theoretical analysis in Sec. III (**Please refer to Supplementary Video**). The 1.25× prototype also demonstrates motion in some compressed states under this magnetic field. However, the 1.00× prototype can only move under this field when uncompressed.

B. Additional Experiments

The ability of the CMCR to move through sections of varying diameter is tested using a tapered tube made from silicone (Fig. 5a). The inner diameter of the tube changes from 26 mm to 21 mm over a length of 100 mm. The 1.25× scale prototype is moved forward and back through the tube, but the motion is restricted partway along the length.

Since the intended application is cardiovascular interventions, the motion of the CMCR in flowing liquid is also tested. Water with red dye is used as the liquid, and the setup is connected to a pump that cycles the water at 2.9 L/min, flow rate of blood through the abdominal aorta. The 1.00× scale prototype is tested in a tube with inner diameter 21 mm in the uncompressed state (Fig. 5b). The CMCR holds steady in the flowing water, and only moves when the rotating magnetic field is applied. Additionally, it does not block the flow of liquid.

In order to demonstrate an approach for minimally invasive insertion of the CMCR, the 1.25× scale prototype is fully compressed and embedded in a block of ice with an outer diameter of 20 mm. It is then inserted through a tube of inner diameter 21 mm and guided to a larger tube with a diameter of 26 mm using a magnet (Fig. 5c). Once at the target location, the ice capsule is melted with water, which releases the flexures and causes the CMCR to anchor in place within the larger tube (Fig. 5d).

V. Discussion

The experimental results show that the CMCR is able to move through both straight and curved tubes in both compressed and uncompressed states. However, the motion is more difficult when the diameter of the tube decreases due to increased friction. This is observed in the experiments in BigMag where the stiffer 1.00× prototype can only produce limited motion under a uniform 50 mT field. The handhled magnets can produce fields up to 100 mT, which is demonstrated to be sufficient to move all three prototypes.

Friction with the vessel wall is one of the primary design considerations for the CMCR. With decreasing vessel diameter, the flexures are compressed more, which causes increase in reaction forces with the wall and consequently friction. The friction is beneficial in ensuring the capsule stays in place under fluid flow or other disturbances. However, increase in friction also leads to increase in actuation magnetic torque needed to generate rotational motion. The dimensions and material of the flexures determine the compression stiffness of the CMCR and therefore the friction force. In this study, the design was limited by fabrication constraints imposed by 3D printing, but it can be improved with a customized fabrication protocol. Increasing the size or volume of the permanent magnets on the CMCR will also help increase actuation torque.

Slippage of the CMCR is observed occasionally in both compressed and uncompressed tests. This undesirable slippage occurs due to attractive forces from the external permanent magnet. This issue can be overcome using an actuation system which can generate a more uniform magnetic field. Excessive axial bending of the CMCR (from the soft material core) is also observed during actuation, which limits the efficiency of motion. While axial flexibility is necessary for navigating bends, it must be optimized for ideal performance. This can be achieved by altering the dimensions or material of the flexible core.

VI. Conclusions & Future Work

In this paper, a combination of flexures, soft materials and magnets are used to design a capsule robot (CMCR) with a flexible structure that can be controlled wirelessly. The CMCR moves through curved and straight tubular structures using screw-like motion under actuation from a rotating magnetic field. The actuation field can be calculated using the stiffness of the flexures. The CMCR can also move through tubes with varying diameters and in an environment with flowing liquid. The 1.00× scale prototype presented here is suitable for the abdominal aorta, with an uncompressed outer diameter of 20 mm. The maximum possible diameter change of the CMCR for all three scaled prototypes is 25%. which may be improved with a smaller core.

The experiments with fluid flow and minimally invasive insertion of the CMCR suggest potential for clinical application. However, this requires further optimization of the design in terms of materials and dimensions. Improved fabrication techniques can help produce parts at smaller scales and with better resolution. The compliance of the flexures must be tuned for suitability in real blood vessels. For use in robotic surgery, the CMCR must also be embedded with sensors and surgical tools. The CMCR can provide a template for wireless robots that can serve surgical applications such as diagnostic imaging and artherectomy.

References

[1] J. Wickham, "Minimally Invasive Surgery," *Journal of Endourlogy*, vol. 1, no. 2, pp. 71–74, 1987.

[2] R. Beasley, "Medical Robots: Current Systems and Research Directions," *Journal of Robotics*, vol. 2012, pp. 1–14, 2012.

[3] Vitiello *et al.*, "Emerging robotic platforms for minimally invasive surgery," *IEEE Reviews in Biomedical Engineering*, vol. 6, pp. 111–126, 2013.

[4] Sitti *et al.*, "Biomedical Applications of Untethered Mobile Milli/Microrobots," *Proceedings of the IEEE*, vol. 103, no. 2, pp. 205–224, 2015.

[5] Burgner-Kahrs *et al.*, "Continuum Robots for Medical Applications: A Survey," *IEEE Transactions on Robotics*, vol. 31, no. 6, pp. 1261–1280, Dec. 2015.

[6] Thomas *et al.*, "Surgical Applications of Compliant Mechanisms: A Review," *Journal of Mechanisms and Robotics*, vol. 13, no. 2, p. 020801, 2021.

[7] Runciman *et al.*, "Soft Robotics in Minimally Invasive Surgery," *Soft Robotics*, vol. 6, no. 4, pp. 423–443, 2019.

[8] Bedell *et al.*, "Design optimization of concentric tube robots based on task and anatomical constraints," *Proceedings - IEEE International Conference on Robotics and Automation*, pp. 398–403, 2011.

[9] Jeon *et al.*, "A Magnetically Controlled Soft Microrobot Steering a Guidewire in a Three-Dimensional Phantom Vascular Network," *Soft Robotics*, vol. 6, no. 1, pp. 54–68, 2019.

[10] Nelson *et al.*, "Microrobots for Minimally Invasive Medicine," *Annual Review of Biomedical Engineering*, vol. 12, no. 1, pp. 55–85, 2010.

[11] Iddan *et al.*, "Wireless capsule endoscopy," *Nature*, vol. 405, no. 6785, pp. 417–418, May 2000.

[12] Singeap *et al.*, "Capsule endoscopy: The road ahead," *World Journal of Gastroenterology*, vol. 22, no. 1, pp. 369–378, Jan. 2016.

[13] Ciuti *et al.*, "Frontiers of robotic endoscopic capsules: a review," *Journal of Micro-Bio Robotics*, vol. 11, no. 1-4, pp. 1–18, Jun. 2016.

[14] A. Mahoney and J. J. Abbott, "Five-degree-of-freedom manipulation of an untethered magnetic device in fluid using a single permanent magnet with application in stomach capsule endoscopy," *The International Journal of Robotics Research*, vol. 35, no. 1-3, pp. 129–147, 2016.

[15] Zhao *et al.*, "Screening for gastric cancer with magnetically controlled capsule gastroscopy in asymptomatic individuals," *Gastrointestinal Endoscopy*, vol. 88, no. 3, pp. 466–474, Sep. 2018.

[16] Ernst *et al.*, "Initial experience with remote catheter ablation using a novel magnetic navigation system: magnetic remote catheter ablation," *Circulation*, vol. 109, no. 12, pp. 1472–1475, 2004.

[17] Gildea *et al.*, "Electromagnetic navigation diagnostic bronchoscopy: a prospective study," *American Journal of Respiratory and Critical Care Medicine*, vol. 174, no. 9, pp. 982–989, 2006.

[18] Hu *et al.*, "Small-scale soft-bodied robot with multimodal locomotion," *Nature*, vol. 554, no. 7690, pp. 81–85, 2018.

[19] Venkiteswaran *et al.*, "Tandem actuation of legged locomotion and grasping manipulation in soft robots using magnetic fields," *Extreme Mechanics Letters*, vol. 41, p. 101023, 2020.

[20] Lu *et al.*, "A bioinspired multilegged soft millirobot that functions in both dry and wet conditions," *Nature Communications*, vol. 9, no. 1, p. 3944, 2018.

[21] Son *et al.*, "Magnetically Actuated Soft Capsule Endoscope for Fine-Needle Biopsy," *Soft Robotics*, vol. 7, no. 1, pp. 10–21, 2020.

[22] Yim *et al.*, "Biopsy using a magnetic capsule endoscope carrying, releasing, and retrieving untethered microgrippers," *IEEE Transactions on Biomedical Engineering*, vol. 61, no. 2, pp. 513–521, 2014.

[23] Pham *et al.*, "Soft Endoluminal Robots Propelled by Rotating Magnetic Dipole Fields," *IEEE Transactions on Medical Robotics and Bionics*, vol. 2, no. 4, pp. 598–607, 2020.

[24] Popek *et al.*, "Six-Degree-of-Freedom Localization of an Untethered Magnetic Capsule Using a Single Rotating Magnetic Dipole," *IEEE Robotics and Automation Letters*, vol. 2, no. 1, pp. 305–312, 2017.

[25] Nam *et al.*, "Magnetic helical robot for targeted drug-delivery in tubular environments," *IEEE/ASME Transactions on Mechatronics*, vol. 22, no. 6, pp. 2461–2468, Dec. 2017.

[26] V. Venkiteswaran and H. J. Su, "Pseudo-rigid-body models for circular beams under combined tip loads," *Mechanism and Machine Theory*, vol. 106, pp. 80–93, 2016.

[27] Sikorski *et al.*, "Introducing BigMag - A novel system for 3D magnetic actuation of flexible surgical manipulators," *Proceedings - IEEE International Conference on Robotics and Automation*, pp. 3594–3599, Jul. 2017.